Article

JOURNAL OF COMPOSITE MATERIALS

Journal of Composite Materials
2021, Vol. 55(20) 2793–2806

DOI: 10.1177/0021998321995912
journals.sagepub.com/home/jcm
SAGE

New fabricated PMMA-PVA/graphene oxide nanocomposites: Structure, optical properties and application

Mohammed Abdul Kadhim[1,2] and Ehssan Al-Bermany[1]

Abstract

Graphene oxide nanosheets (GO) bring more interest in the tunable bandgap and enhanced the optical properties of nanocomposites. The developed method successfully mixed the PMMA- dissolved in dimethylformamide (DMF) with PVA dissolved in distilled water (DW) and DMF. New (PMMA-DMF)-(PVA-DW-DMF)/GO nanocomposite was successfully fabricated with various loading ratios of GO nanosheets for the first time. Several factors were applied to get fine desperation and homogeneous using the acoustic-solution casting method. Optical Microscope (OM), Fourier-transform infrared spectroscopy (FTIR), X-ray diffraction (XRD), and UV–visible spectrophotometer were applied to investigate the structure and optical properties of the PMMA-PVA-GO nanocomposite. The OM images confirmed the fine homogenous matrix and GO distribution in the nanocomposites. FTIR spectra exhibited the most functional group of polymers and GO in the nanocomposites and strong interfacial interaction between the GO and matrix as confirmed by the shifting in the XRD patterns of the PMMA. The optical properties results of the PMMA-PVA/GO nanocomposites revealed an improvement up to 400% of the absorbance, 337% of the absorption coefficient, 51% of the refractive index, 210% of the real and 125% of the imaginary dielectric constants in terms to increase the GO concentrations, whereas the reduction in the transmittance and energy bandgap results of allowed and forbidden indirect transition were exhibited up to 9 and 16.4%, respectively. These results could grow for better and wide applications such as radiation shielding, specific optoelectronic applications, and filters ultraviolet also could use in landfilling the chemical, nuclear, and radioactive waste.

Keywords

Graphene oxide, PMMA, PVA, optical properties, nanocomposites, radiation absorption

Introduction

Nanocomposites are an essential topic of polymer-nanomaterials that have been developed and demonstrate distinct physicochemical properties.[1,2] The interfacial interactions and fine dispersion of nanofiller with the polymer in the nanocomposites are considered the most important factors that result in impartment improving in the properties of nanocomposites,[3–5] where the properties of polymers improve and hence this has achieved, a lot of applications depend upon the contribution of the nanomaterial in the polymers.[6,7] Recently, one of the best potential nanofillers is graphene[8,9] which has the best mechanical properties,[10] high conductivity,[11,12] transparency[13] and tunable the bandgap,[14] etc. These unique properties make graphene an excellent applicant to use in many substantial applications, for instance, transparent electronics,[15] solar cells[8] as well as sensors,[16] etc.

PMMA is a transparent polymer, durable, and environmentally stable, etc. These features make it a good candidate to use in a wide-ranging of applications, for instance, vehicle appliances, commercial aquariums, lenses for glasses, and TV screens, etc..[17] Moreover, It is the preferred material by researchers and engineers

[1]Department of Physics, College of Education for Pure Sciences, University of Babylon, Iraq
[2]Educational Directorate of Babylon, Ministry of Education, Iraq

Corresponding author:
Ehssan Al-Bermany, Department of Physics, College of Education for Pure Sciences, University of Babylon, Iraq.
Email: ehssan@itnet.uobabylon.edu.iq

for outdoor applications, additionally, PMMA has easily hydrolyzed ester groups that make it a poor resistance to several chemicals.[18] Therefore, researchers reported blend PMMA with several materials to improve its properties. They use different methods, polymers and nanofillers for modifying the electrical[19] mechanical,[20] thermal stability[21] and other properties[2] of PMMA for use in a wider range of applications, whereas only two investigations[22,23] focused on the optical properties of PMMA-PVA blend. On the other hand, poly(vinyl alcohol) (PVA) is a synthetic polymer, odorless, translucent, tasteless, or cream-colored granular powder.[24] PVA has good properties that are distinguished from other polymers such as strength, corrosion resistance, and good thermal stability.[19] It contains a carbon chain backbone fastened to methane carbons with hydroxyl functional, which is considered the source of hydrogen bonding that helps to form polymer mixtures.[25,26] Many researchers have investigated the PVA use as fillers or cross-linked products, also it has been widely applied to manufactured nontoxic, harmless and living tissues, etc. as a thermoplastic polymer.[27,28] Additionally, nanoparticles could physically entangle or chemically bound with PVA.[29] It is widely used in making paper and textile industries in the manufacture of membranes resistance to oxygen in the coating photographic film.[30] Therefore, PVA is used to improve the cross-linked between PMMA and graphene nanosheets as well as to improve other properties of the nanocomposites in these investigations.

Many studies[2,22,23,31–33] reported very interesting results when PMMA with PVA polymers were composed together as blended polymer or with other nanoparticles. Linking these polymers together with graphene has not been addressed before to the best of our knowledge. Therefore, this study aims to investigate the new combination, which could bring significant attention and open new approaches for several applications. Where Yakuphanoglu and Erten[23] reported the preparation of PMMA-PVA thin films applying UV-VIS spectrum measurements to study the refractive index behavior. Chloroform was used to dissolve both polymers under stirring for 48 h at room temperature. The results presented the same pattern of the real dielectric constant (E_r) and imaginary (E_i) part, whereas the values of the E_r are higher than E_i. At high frequency, the results were close to both dielectric constant $\varepsilon_{\infty(1)}$ and $\varepsilon_{\infty(2)}$. Tripathi et al.[22] used the solution casting technique to blend PMMA and PVA and characterized their optical properties. Where PMMA was dissolved in benzene and PVA was dissolved in distilled water. The addition of the PVA of the PMMA matrix modified the optical properties of PMMA in the matrix and vice versa was right. They studied the impact of ratio on these polymer properties. FTIR results presented a modification in positions and intensity of the most peak that could provide strong evidence of good interaction and modification of the bond between these polymers. The edge of absorption was shifting to higher energies and bandgap. The findings confirmed the significant effect of the concentration of polymers as functional properties of polymers.

Other researchers[2,31,32] reported the contribution of graphene on the range of the properties of the PMMA or PVA but all these investigations studied these polymers in terms of the difficulty of mixing these polymers together according to their solvent's. It is hard to get a homogenous matrix without aggregation. The information about mixing these two polymers still needs more investigation to reduce the knowledge gap about blending these materials. Zhao et al.[31] described the purification of graphene-based PVA composites to develop the properties of the composite, such as mechanical and thermal properties. SDBS solution was used to disperse the GO using sonication. The GO/PVA composites were homogeneous dispersion. Mechanical properties of the samples exhibited improvements, such as up to 150% and 10 times the higher tensile strength and Young's modulus, respectively. This was achieved in terms of the contribution of 1.8% vol from graphene in the matrix. Yang et al.[2] reported the preparation of PMMA/graphene and GO applying self-assembly methods. The incorporation of both graphene and GO nanosheets provided an important reinforcement for the composites. This contribution was presented with a rise in the value of the PMMA results, such as the modulus of storage as well as the glass transition. Recently investigation[32] reported the preparation of PMMA/GO nanocomposite and PMMA/GO-Fe3O4 for adsorption and removing the malachite green (MG) dye. The adsorption is exothermic in nature form the calculation values of the Gibbs energy (ΔG°), entropy (ΔS°), and enthalpy (ΔH°). The results showed that 35 min was the best contact time to adsorb the MG dye on both nanocomposites from the aqueous solution.

Despite all the above studies, only a few studies[2,31–33] reported the effect of graphene on only PMMA or PVA separately. This is the first investigation that has reported the effect of GO on the successful preparation of PMMA-DMF with PVA-DW-DMF nanocomposites using the developed mixing-sonication-acoustic method. Where the fine homogeneous mixture got between the polymers and fine dispersion of the GO in the matrix. The PVA was used with a low loading ratio to improve the properties of PMMA and increased the cross-linked between PMMA and graphene nanosheets as well as to improve other

properties of the nanocomposites in this investigation. These nanocomposites have characterized the effect of graphene oxide nanosheets on some of the optical properties using FTIR, OM, UV–visible spectrophotometer, and using to absorption the radiation for shield application.

Experimental part

Materials

Polymethyl methacrylate (PMMA) with a (20,000–18,000 g/mol) molecular weight with 213°C melting point and 99% purity was purchased from Tuttlingen Company. The poly (vinyl alcohol) with molecular weight (18,000–12,000 g/mol), melting point of 230°C, and 99% purity was provided by the Panreac Company, Spain. Sodium nitrate ($NaNO_3$), graphite powder ($\leq$39 µm), potassium permanganate ($KMnO_4$), hydrochloric acid (35%), sulfuric acid (H_2SO_4) (analytical grade, 99.5%), and hydrogen peroxide were supplied by Sigma-Aldrich, UK.

Synthesis of graphene oxide

GO nanosheets was predicated by our group that described in details in the previous publications,[34,35] where the size of GO nanosheets was between 94.49 nm to ~2 µm of the surface area and 0.700 nm of the thickness as presented in Figure 14(e), (f), and (h) and Figure S1(d), respectively. For more details, see the SI for the full characterizations of the GO nanosheets.

Purification of the nanocomposites. The various ratio of PMMA-DMF and PVA-DW/DMF was applied to get the appropriate methods to mix these two polymers with different solvents. We reported the methods that accessed not only mixed two of these polymers with their different solvent but also got a fine homogeneous matrix with good GO dispersion and without any aggregation. First, 1 g of PVA was dissolved in 50 ml DW under stirring for 1 h 80 ± 3°C, meanwhile, PMMA was dissolved in DMF with 6 g in 50 ml (DMF) using a magnetic stirrer for 3 h at 80 ± 3°C. At the same time, GO nanosheets were dispersed in DMF with 0.09–0.27 wt.% in 50 ml using a magnetic stirrer and sonication bath as an acoustic solution method for good dispersion of GO in the solvent. All these steps were carried out separately before mixing the materials. Secondly, after the complete dissolve of the PVA in DW, 10 ml of DMF were added to 30 ml of PVA-DW solution then were mixed using magnetite stirrer for 0.5 h at 80 ± 3°C for better homogenous. Thirdly, 5 ml PVA-DW-DMF were added to 25 ml of PMMA-DMF solution and mixed for 4 h using a magnetic stirrer at 80 ± 3 C° and the polymers matrix was fine homogenous during this time. Then the temperature of the PVA-PMMA matrix was reduced to about 35 ± 3°C before adding three ratios of GO-DMF to prepare three nanocomposites. After the addition of GO, the mixing-sonication methods were applied. Where the mixing of the PVA-PMMA/GO matrix was continued for another 3 h then it was sonicated for 15 min and repeat this procedure four times to get fine homogenous and dispersion of GO in the polymers matrix. Figure 1 and Table 1 demonstrate the summarization of the fabrication method.

Characterization. Nikon – 73346, Optical Microscope (OM) with light intensity and automatically controlled camera and different magnification that was used to characterize the samples and supplied from Olympus.

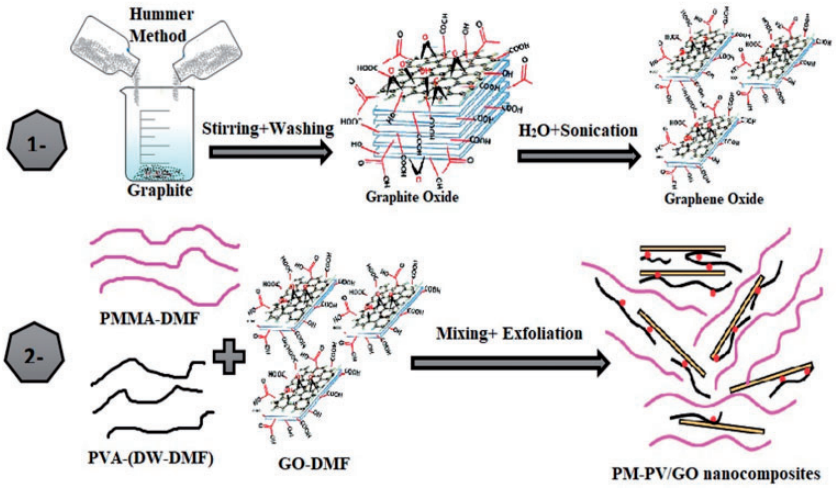

Figure 1. Schematic of synthesis of GO, PM-PV1, and PM-PVGO nanocomposites.

Table 1. The purification method of samples.

	Concentration (wt. %)			Total time (h)		
Sample ID	PVA	PMMA	GO	Sonication	Mixing	Drying method
GO	0	0	100	0.4	4	Freeze drier
PM-PV1	4	96	0	0	4	40 ± 3°C under air
PM-PVGO2	3.91		0.09	0.45	12	
PM-PVGO3	3.82		0.18	1	12	
PM-PVGO4	3.73		0.27	1.15	12	

Vertex 701 Fourier transforms infrared (FTIR) spectra from Bruker Company, Germany, were used to characterize the nanocomposites in the region between 4000 and 400 cm^{-1}. Shimadzu UV-1650, UV-visible spectrophotometer from Phillips a Japanese company has characterized the nanocomposites in the range between 200 and 1100 nm wavelengths. CO^{60} with five MCI activity was used to characterize the influence of the ratio of GO in the nanocomposites for shielding applications. The source was placed away 3 cm from the detector of the Geiger counter, meanwhile, the samples were pleased away 2 cm from the radiation source. XRD diffraction device type (SHIMADZU 6000) made by the Japanese company was used to characterize the crystal structures of all samples. Scanning electron microscopy (SEM) made by FEI Company type Inspect F, which was used to characterize the nanocomposites at voltage 10 kV.

Theoretical part

The ratio between the intensities of the absorbed light (I_A) and the incident light (I_o) of materials can be defined as the absorbance (A) that is given in the following equation (11)

$$A = \log T \tag{1}$$

From the below relationship, the transmittance spectra (T) is calculated[11]

$$T = \frac{I_A}{I_0} \tag{2}$$

From the Lambert bear formula, the absorption coefficient (α) $(cm)^{-1}$ is considered[36]

$$\alpha = 2.303 \ A/t \tag{3}$$

The thickness (t) of the samples, allowed and prohibited indirect of the optical energy gap of PMMA-PVA and PMMA-PVAGO nanocomposites were calculated using formula[4] from both the interception of the extrapolated linear part beside the energy of the photon ($h\upsilon$) at $(\alpha h\nu)^{1/n} = 0$[37]

$$ahv = B\ \left(hv - E_g\right)^n \tag{4}$$

where (B) is a constant, (v) is the frequency, (h) is Planck's constant, (E_g) is the phonon energy, and (n) is the constant of the exponential, which depends on the transition type; r could represent in many values as 1/2 and 3/2 or 2 and 3 for the direct allowed and forbidden or indirect allowed and bidden, respectively.[38,39] The index of refractive (n) is calculated according to the equations as well as the coefficient of extinction (k)[38]

$$n = \frac{1+R}{1-R} + \left[\frac{4R}{(1-R)^2} - K^2\right] \tag{5}$$

$$K = \frac{\alpha\lambda}{4\pi} \tag{6}$$

where (λ) and (R) are the wavelength of (Cu Kα) with line (1.5405) Å and the reflectance, respectively. At optical frequencies, it is characterized by the waves of the light, where the electronic polarity is considered as dominating above all other remaining polarization types. Equations (7) to (9) are used to characterize the constant of both real and imaginary dielectric[39,40]

$$\varepsilon = (\varepsilon_r + \varepsilon_i) \tag{7}$$

$$\varepsilon_r = (n^2 - k^2) \tag{8}$$

$$\varepsilon_i = (2nk) \tag{9}$$

where (ε), (ε_r) and (ε_i) mean the dielectric constant, the real part, and the imaginary part of the dielectric constant, respectively. Formulation[10] was applied to calculate the radiation attenuation. The counted number (N) was recorded during the same time and

(x) is the thickness of the sample, (N_o) means the radiation particle number that is counted without any absorber with certain time duration, (μ) means the coefficient of attenuation of gamma radiation. The scattering form of the sides reduces the absorption by Lambert law[41]

$$N = N_o \exp^{(-\mu x)} \quad (10)$$

Results and discussion

Figure 2 illustrates the FT-IR spectrums of GO, PMMA-PVA blend, and PMMA-PVA/GO nanocomposites. It was recorded in the range (4000–500) cm^{-1}. In Figure 2(a), the FT-IR spectrum of GO shows a broadband peak at 3220 cm^{-1} that is associated with the hydroxyl groups (O–H) stretching vibrations. The peak at 1723 cm^{-1}, an adsorption functional group matched to the stretching carbonyl groups (C = O).[9] At 1604 cm^{-1}, this peak is recognized as a skeletal ring (C = C). It is a stretching vibration functional group of the sp^2 carbon domain as un-exfoliated GO sheets. Meanwhile, the functional groups at 1374 and 1040 cm^{-1} are associated with epoxy (C–O–C) and (C–O) groups,[32] respectively.

The PMMA-PVA blend spectra in Figure 2(b) presented several peaks such as, 1646, 1604, 1361, and between 1260 and 1000 cm^{-1} that were attributed to (CH_2), (C–H) stretching, (O–H) bending, and (C–O) (ester bond) stretching vibration. These functional peaks were related to functional groups peaks of both PMMA,[42] and PVA[43] net. The contribution of the GO has presented a new functional peak in the nanocomposites, as displayed in Figure 2(c) to (e). Where the samples observed new strong bands at 2904, 1604, and 887 cm^{-1}. Additionally, it revealed an increase in the intensity of other peaks with the increase of the contribution of GO in the nanocomposites. Moreover, increasing the ratio of the GO to 0.27 wt%, which is the highest ratio in this investigation, resulted in shifting in functional peaks of PM-PVGO4 up to 10 cm^{-1} to most functional groups in addition to increase the intensity peaks because the addition of the nucleating agent PMMA-PVA/GO.

From the infrared spectra, it can be noticed that the intermolecular interaction of the carbonyl group in PMMA with the OH group in PVA.[20] These results present the significant modification of PMMA made by PVA compared to PMMA in agreement as reported in the literature.[44] Additionally, the variation of (GO) nanoparticles ratio causes some significant changes and strong interfacial interaction in the spectrum of PMMA-PVA. This can be related to the fact that the

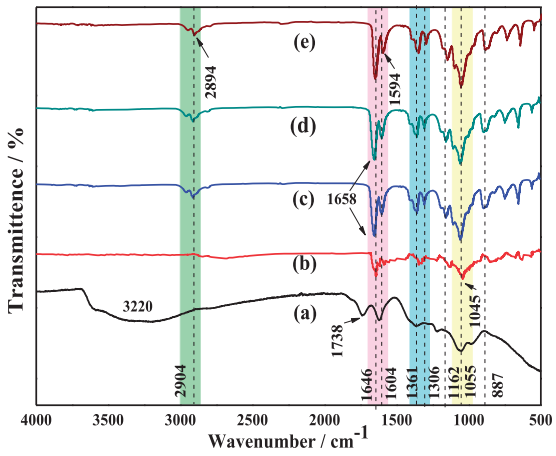

Figure 2. FTIR spectra of (a) GO, (b) PM-PV1, (c) PM-PVGO2, (d) PM-PVGO3, and (e) PM-PVGO4.

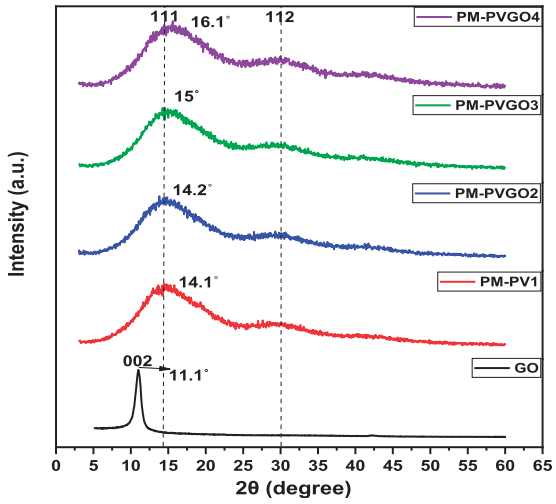

Figure 3. XRD patterns of GO, PM-PV1, and PM-PVGO nanocomposite.

formulation of the hydrogen bonds between the O-H in the GO and the C = O in the PMMA-PVA. Also, this could be related to the charge coming to the other atoms that being separated from the C = O function group. The property of C = O with a double bond led to a reduction of the absorption and shifted the functional peaks to the low wavenumber.[45]

Figure 3 shows the XRD patterns of GO, PM-PV1, PM-PVGO2, PM-PVGO3, and PM-PVGO4 nanocomposites. A strong diffraction peak at $2\theta = 11.1°$ is presented in the XRD spectra. This peak with (002) diffractions is considered to GO nanosheets with interlayer spacing 0.79 nm that was calculated from the Bragg equation. The GO peak was shifted from the at $2\theta = 26.5°$ of graphite, this shifting confirmed the oxidation of flakes and produced of GO nanosheets in agreement with the literature,[2,46] also see Figure 1S.

PM-PV1 pattern exhibited two broad peaks at $2\theta = 14.1^\circ$ and 30°, which are related to (111) and (112) diffractions that related to the PMMA in agreement with the literature.[2,47] Both patterns of the GO at $2\theta = 11.1^\circ$ and PVA at $2\theta = 19.8^\circ$ were located in the wide and high-intensity pattern of PMMA that between 7° and 23°. Therefore, the peaks of GO and PVA could overlap with PMMA and also the full desperation of GO nanosheets in the matrix illustrated clearly in the OM images or because of orientation, in agreement with the literature,[48] that makes it is difficult to present in the XRD patterns even in the samples. Whereas, the influence of increasing the ratio loading of GO nanosheets in the matrix presented shifting in peaks of the PMMA. Where the PMMA peak slightly shifted from $2\theta = 14.1^\circ$–14.2°, 15°, and 16.1° with the increase of the loading ration of GO nanosheets from 0 wt% to 0.09, 0.18, and 0.27 wt% in the matrix of the PM-PVGO2, PM-PVGO3, and PM-PVGO4, respectively. This shift could refer to the increment of interplanar crystal spacing and observed the volume expansion in the macro.[49] The XRD finding has supported the finding of the FTIR spectra that showed a strong interaction between the nanosheets and matrix, also it significant showed that the GO nanosheets did not affect the crystal structure of the polymers in the nanocomposites in strong agreement with the literature.[11,49] Where the interplanar d-spacing was calculated from the position of the (111) peak using the Bragg equation[50]

$$n\lambda = 2d\sin(\Theta) \tag{11}$$

where (n), (λ), (d), and (θ) mean the integer, the wavelength of the incident X-ray, d-spacing, and angle between the incident beam and scattering plane, respectively. Meanwhile, the crystallite size (D) was estimated from the Scherrer formula[51]

$$D = \frac{K\lambda}{\beta\cos(\theta)} \tag{12}$$

where (K) and (β) are the shape factor for the average crystallite ($\sim$0.9), and the full width of materials peak at half-maximum (FWHM). The d-spacing and crystallite size of PM-PV1 and PM-PV/GO nanocomposite are demonstrated in Table 2. In Table 2, the results of the nanocomposites revealed only a slight reduction of the d-spacing because of the contribution of GO nanosheets. Meanwhile, the same behavior was exhibited with the average crystallite size of nanocomposites that also slightly decreased compared to the blended polymer PM-PV1. In general, the optical properties of samples were positively influenced by their crystallinity and crystallite size.

Table 2. Summarized the lattice spacing, FWHM (β), diffraction angle, and the average crystallite size of PM-PV1 and PM-PV/G nanocomposite.

Samples	*d*-Spacing (A)	β (°)	θ (°)	D (A)
PM-PV1	0.627	10.05	7.05	7.96
PM-PVGO2	0.622	10.9	7.1	7.34
PM-PVGO3	0.589	11.05	7.5	7.24
PM-PVGO4	0.549	11.1	8.05	7.22

Figure 4 displays the optical absorbance in the range (300–1100 nm) wavelength of PMMA-PVA blend and PMMA-PVA/GO nanocomposites. All the measurements were carried out using a spectrophotometer with a double-beam of the films at room temperature. Figure 4 reveals that the value of all samples displays high absorbance in the region of ultraviolet in comparison with the PM-PV1 film. The blend of the PM-PV1 film absorbance about 0.6 from the photons at 260 nm. Where, at these energies, the donor electrons were excitations to the conduction band, where absorbing a photon of known energy by the electron resulted exciting in these electrons from a lower to higher energy level. Besides, the results showed a high absorbance photon by the samples at the UV region. This led to attribute enough energy of these photons to interact with atoms. In the absorbance spectra, the fundamental absorption could indicate the excitation transition or the band, where the types of possible transitions of the electron can understudy from the changes in the transmitted and absorbed.[52] Additionally, the absorbance was enhanced by increasing the contribution ratio of the GO nanosheets. Interestingly, the contribution of the GO nanosheets raise the absorption of the photon to greater than 1, this means, more than 90% of the photons were absorbed by the nanocomposites. Where graphene nanosheets have high absorbance for each nano-flack could reach 2.3% of the light over a broad wavelength range, which makes it suitable for specific optoelectronic applications.[53] Where graphene increased the absorption of the incident light by free electrons. Here the interaction between materials with incident photon will present. The increase in the nanoparticle concentration with fine distribution in the matrix was responsible for the increase in the charge carrier's number[54] in agreement with finding results reported in the literature.[54,55] GO has many chemical reactive sites with free energy in the polymer chains, which has led to strong hydrogen bond interaction between the polymer and GO nanosheets. The hydrogen bond is considered another factor in increasing the absorption in the nanocomposites.[56] Whereas, in the

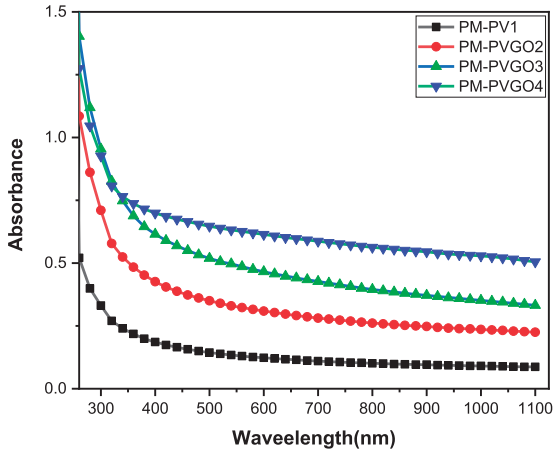

Figure 4. The absorbance spectra with the wavelength of PM-PV1 and PM-PVGO nanocomposite.

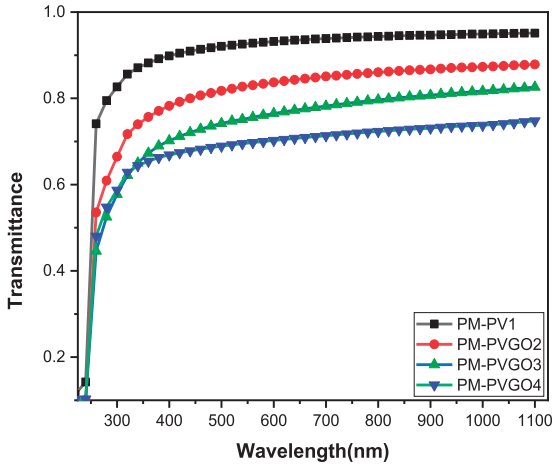

Figure 5. The transmittance spectrum with a wavelength of PM-PV1 and PM-PVGO nanocomposite.

visible region, all nanocomposites value illustrated low absorbance. Where this could be related to the incident photons cannot interact with atoms because it does not have enough energy at a high wavelength, as well as the photon, was transmitted.[57] At 600 nm, the presented results indicated a significant improvement in absorbance up to 150, 280, and 400% with the increase of concentrations ratio of GO by 0.09, 0.18, and 0.27 wt. % in the nanocomposites, respectively. These findings align with the literature.[14,43] Additionally, GO has many chemically reactive sites with free energy in the polymer chains that led to strong hydrogen bond interaction between the polymer and GO nanosheets. The hydrogen bond is considered another factor that increases the absorbing ratio of the light.

Figure 5 demonstrates the transmittance (T) spectrums with the wavelength of the PM-PV1 and PM-PVGO nanocomposites. The figure indicates that the transmittance for all samples has increased rapidly with an increasing wavelength around 240 nm and the increase was almost steady after 260 nm. The findings were clearly showing the contribution of the GO reduced the light transmittance. This behavior was increased by increasing the contribution ratio of the GO in the matrix, where increasing the nanomaterials could lead to increasing the absorbance of light and reducing the transmittance for the same reason.[58] At 600 nm, the results displayed a reduction in transmittance results to 10, 18, and 23% with increasing the ratio of GO up to 0.09, 0.18, and 0.27 wt.%, respectively, in the polymer matrix.

The absorption coefficient α of PM-PV1 and PM-PVGO nanocomposite films with the energy of the photon is shown in Figure 6. The behavior of the absorption coefficient exhibited steady growth in

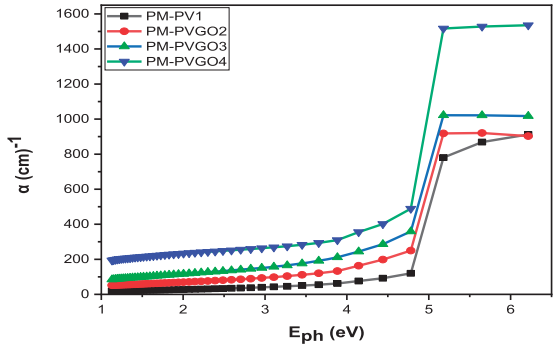

Figure 6. The coefficient of absorption with the energy of a photon of PM-PV1 and PM-PVGO nanocomposite.

the values with increasing the energy of photon until the value at 4.8 eV. This could be related to the lower transition of the electron, were in this area, the incident photon energy was not enough for moving the electron toward the conduction band from the valence band. Whereas, after 4.7 eV, the coefficient of absorption showing a rapid increase of all sample results due to the great transitions of the electron for the conductive band.

At (4.5 eV), the results indicated a significant enhancement in absorption coefficient up to 116, 212, and 337% with increasing the contribution of graphene oxide concentrations in the nanocomposites up to 0.09, 0.18, and 0.27 wt.%, respectively.

Figures 7 and 8, illustrate the absorption edge for the allowed $(\alpha h\upsilon)^{1/2}$ and forbidden $(\alpha h\upsilon)^{1/3}$ indirect transition respectively, of PM-PV1 and PM-PVGO with the photon energy. The intercept of the extrapolated linear part was used to estimate these values at $(\alpha h\upsilon)$ $n = 0$. At the value $(\alpha h\upsilon)^{1/2} = 0$, and to calculate

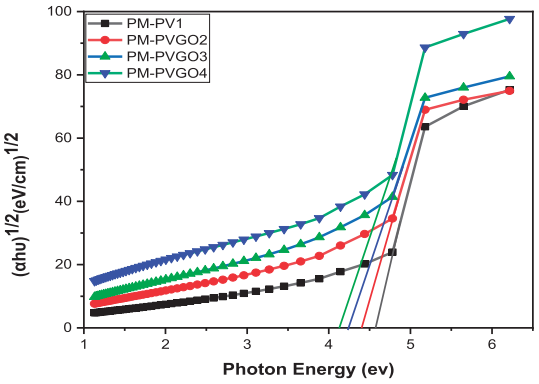

Figure 7. Optical energy gap for the allowed indirect transition with the energy of a photon of the PM-PV1 and PM-PVGO nanocomposite.

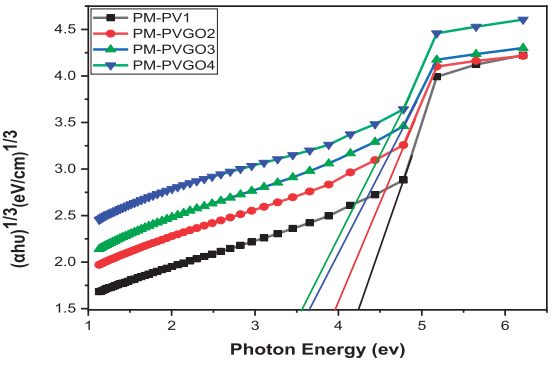

Figure 8. Optical energy gap for the forbidden indirect transition with the photon energy of PM-PV1 and PM-PVGO nanocomposite.

the energy gap, drawing a straight line from the upper part of the curve in Figure 7 to the (x) axis for the allowed indirect transition as well as the same procedure was followed to estimate the forbidden indirect transition in Figure 8.

At (4.8 eV), the results exhibited an important improvement in the energy gap values of the allowed and forbidden indirect transition up to 45, 73 and 9% and 13, 20 and 27% of the samples respectively, with the rise of the GO ratio contribution by 0.09, 0.18 and 0.27 wt.% in the nanocomposites. The results of the energy gap of both allowed and forbidden indirect transitions were reduced up to 9% as well as 16.4%, respectively, as shown in Table 3, where the contribution of GO presented a significant effect on the tunable bandgap as well as increasing the loading ratio of GO.[14] This led to an important reduction in the values of the energy gap of nanocomposites.

Table 3. Summarized the optical energy gap of PM-PV1 and PM-PV/G nanocomposite.

	Indirect transition (eV)	
Samples	Allowed	Forbidden
PM-PV1	4.58	4.25
PM-PVGO2	4.4	3.91
PM-PVGO3	4.25	3.65
PM-PVGO4	4.18	3.55

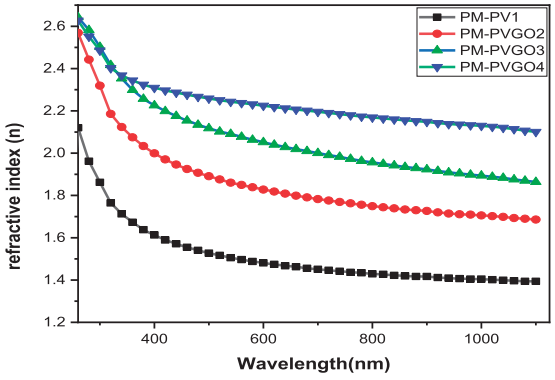

Figure 9. Refractive index with a wavelength of PM-PV1 and PM-PVGO nanocomposite.

Figure 9 illustrates the refraction index curves of PM-PV1 and PMMA-PVA/GO nanocomposites with the wavelength. The refractive index of the samples improved with the incorporation of GO nanosheets in the nanocomposites. This behavior may be attributed to the increase in the density of nanocomposites. At 600 nm, the results displayed significant enhancements in of refraction index up to 24, 39, and 51% with the contribution of graphene oxide increasing the concentrations up to 0.09, 0.18, and 0.27 wt.% in the nanocomposites.

The variation in the real and imaginary dielectric constant with the wavelength of the PM-PV1, and PM-PVGO nanocomposite films are illustrated in Figures 10 and 11, respectively. These figures show that both parts real and imaginary dielectric constants were improved by increasing the ratio of the concentration of GO nanosheets. This is attributed to the increase in electrical polarization in the nanocomposites. At 600 nm, the results exhibited the improving the real and imaginary dielectric constant for two parts were increased up to 25, 71, and 210%, and 53, 92, and 125% respectively, with increasing the concentrations of graphene oxide by 0.09, 0.18, and 0.27% in the nanocomposites.

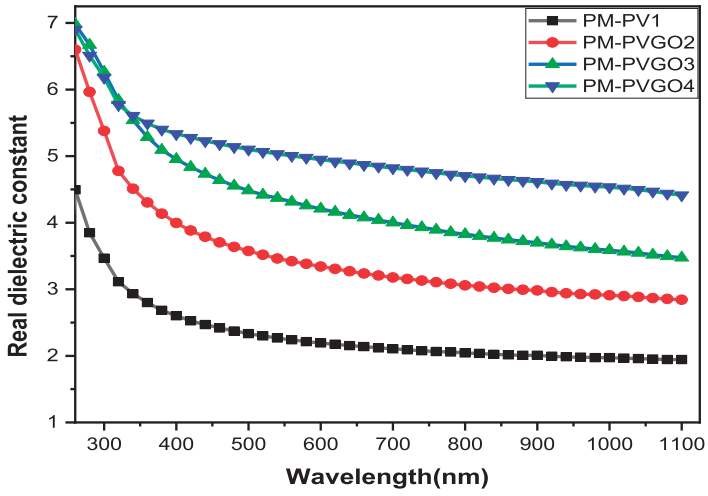

Figure 10. The real dielectric constant with the wavelength of PM-PV1 and PM-PVGO nanocomposite.

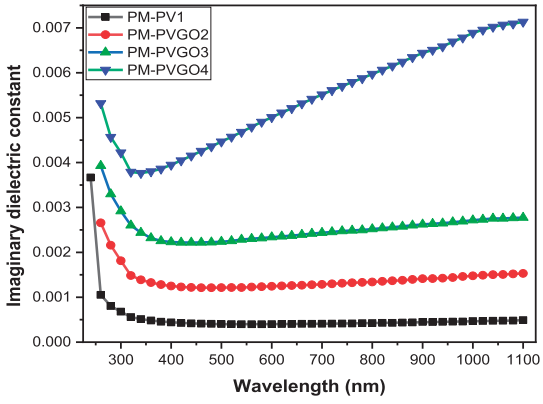

Figure 11. The imaginary dielectric constant with the wavelength of PM-PV1, PM-, and PM-PVGO nanocomposite.

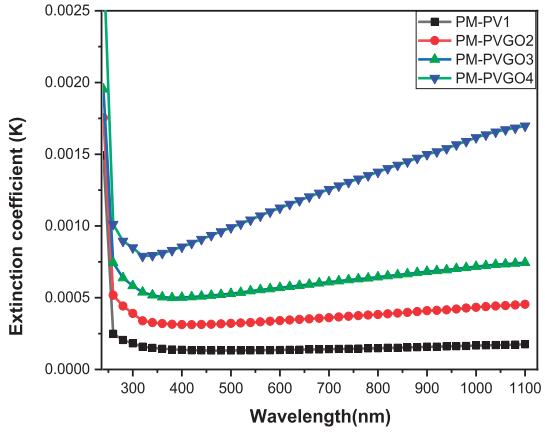

Figure 12. The extinction coefficient with the wavelength of PM-PV1 and PM-PV/GO nanocomposite.

Figure 12 demonstrates the coefficient of extinction (K) with the wavenumber of the PM-PV1 and PM-PVGO nanocomposite films. Where, at the UV region, the extinction coefficient of nanocomposites displayed higher values. This behavior of the extinction coefficient resulted from the high absorbance of all nanocomposites. Also, the same behavior was presented in visible and near-infrared regions. These results presented a significant improvement in the behavior of the nanocomposites due to the incorporation of the GO nanosheets, especially the higher ratio of the GO used in this investigation that demonstrated a general improvement in the results in comparison with other nanocomposites as well as with increasing the wavenumber as clearly shown in Figure 12. At 600 nm, the results indicated important enhancements in of extinction coefficient up to 51, 321, and 732% with the increasing concentrations of graphene oxide by 0.09, 0.18, and 0.27 wt.% in the nanocomposites.

Figure 13 shows the optical images of PMMA-PVA and PMMA-PVA/GO nanocomposites with different concentrations of GO at magnification power ×40. These images illustrated the fine homogeneity of the matrix with a good distribution of GO into the blend-polymer composites. The OM images exhibited a successful preparation of the PMMA-PVA/GO nanocomposites using this method. In comparison among the polymers blending films with PMMA-PVA/GO nanocomposites films, a notable modification with increasing the ratio of the GO was noticed. The contribution of GO exposed many changes in all these films without any aggregations or effect on the transparency of the films. Additionally, the fine distribution considerably got better with the increase of the ratio of

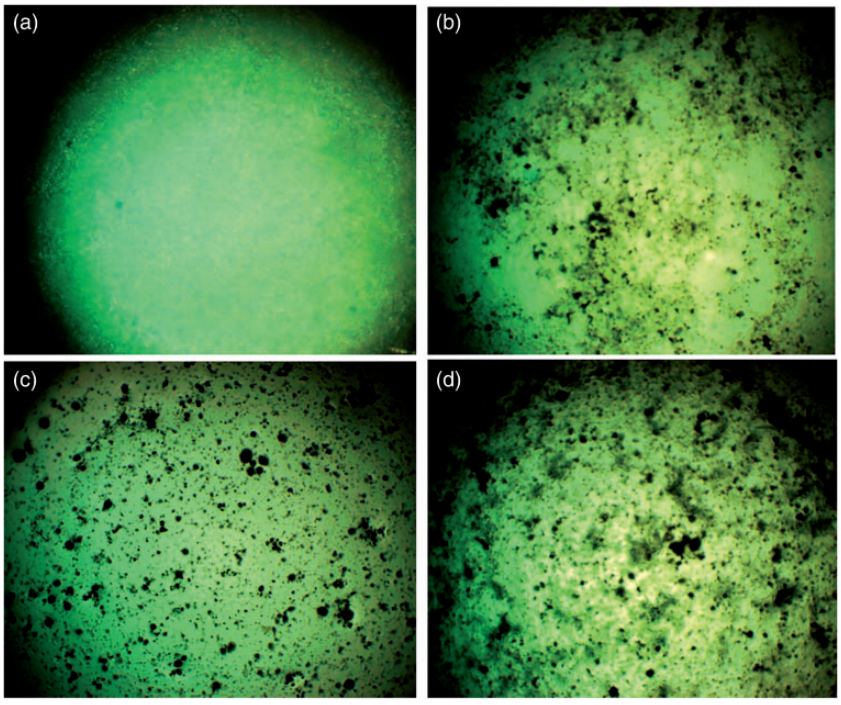

Figure 13. The images of the optical microscopy with a magnification of (40×) of (a) PM-PV1, (b) PM-PVGO2, (c) PM-PVGO3, and (d) PM-PVGO4.

the GO, especially in the sample PM-PVGO4, as illustrated in Figure 13(d) in agreement with other authors finding.[11,59]

Scanning electron microscope is used to investigate the surface morphology of samples and the dispersion of (GO) in the polymers matrix. Figure 14 shows an SEM micrograph of the surface of the (PMMA-PVA) blend and (PMMA-PVA/GO) nanocomposites films. Image (a) in Figure 14 exhibits the blended polymers that found a uniform morphology revealing a rather soft surface. In Figure 14(b) to (d), the increase of the nanosheets ratio of graphene oxide in a polymer matrix for the (PMMA-PVA/GO) nanocomposites led to changes in the morphology of the surface. The nanocomposites films showed many GO nanosheets that were fine dispersion without aggregates with good distribution and spread densely on the surface, this may be indicating the occurrence of a homogeneous growth mechanism. The results agree with optical microscopy images and results from previous investigations.[60] The SEM images (e, f, and h) in Figure 14 illustrated the measurements of GO size that were between a few nanometers to few microns.

The contribution of GO in the nanocomposites illustrated the reduction of the transmission radiation of the nanocomposites as shown in Figure 15. Figure 15 displays the ratio between the radiation attenuation (N) as (N/N0) with the number of radiation particles which is counted during a certain time (N_o) versus the increasing concentrations of GO nanosheets. Where a significant reduction was exhibited with increasing the ratio of GO in the nanocomposites.

PM-PV/GO nanocomposite with a higher ratio of GO reduction increasing the reduction of the value of the (N/N0) ratio as a result of increasing the GO concentration in the nanocomposites compared with PM-PV1. Where, the GO nanosheets reduced the transmission radiation of gamma-ray as well as is responsible to increase in the gamma radiation of coefficients attenuation, where the gamma rays shielding has required materials with large amounts of mass, high density, and high atomic numbers, which are exhibited better shielded due to increasing the total GO nanosheets per area in the gamma rays path. This probability for absorption passed gamma-ray through the nanocomposites leads to an exponential decrease of intensity. These results show a promising ability for these samples to absorb ionizing radiation that opens the wide application in ionizing radiation absorption, such as making suits and special glasses for workers in laboratories containing this type of radiation. Moreover, it could be used as an important component material in the mixture of light concrete that uses in landfilling the chemical nuclear and radioactive waste to increase their effectiveness in absorbing radiation and other important applications in this field.

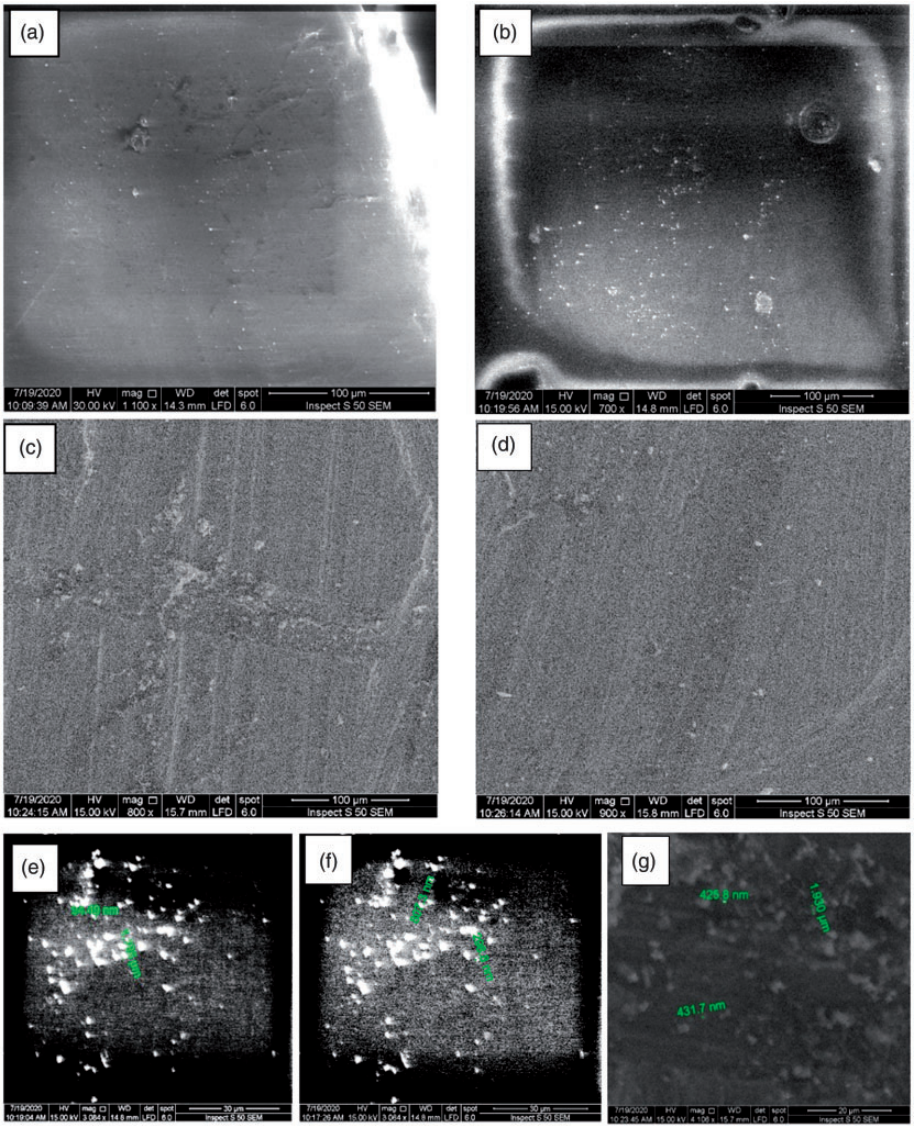

Figure 14. SEM image of (a) PM-PV1, (b) PM-PVGO2, (c) PM-PVGO3, (d) PM-PVGO4 nanocomposite, and (e, f, and h) present the nanosize calculation of GO in nanocomposites.

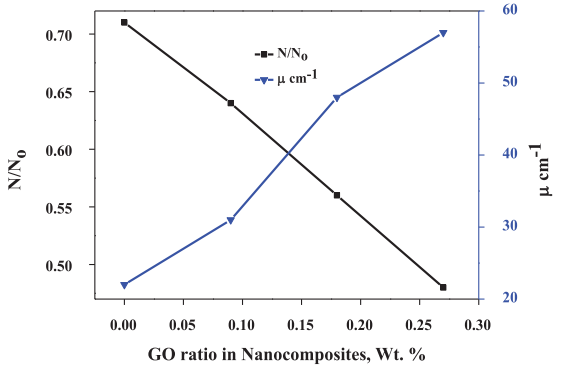

Figure 15. The ratio between the radiation attenuation (N) with the number of radiation particles (N_o) as (N/N_o) and the coefficient of attenuation of gamma radiation with GO ratio of PM-PV1 and PM-PV/GO nanocomposites.

Conclusions

The contribution of GO nanosheets exhibited a strong interfacial interaction that was formed with polymers in the polymer matrix nanofillers as presenting using FTIR and the shifting in the XRD peaks. The contribution of GO illustrated a significant enhancement in the optical properties. This improvement significantly increases with increasing the loading ratio of GO nanosheets in the nanocomposites even at the loading ratio. The fabricated of the new nanocomposites was successfully achieved with a homogenous and fine dispersion of the GO nanosheets in the matrix. Most of the optical properties such as the absorbance, coefficient of absorption, dielectric constant (real and imaginary), and refractive index of PMMA-PVA/GO

nanocomposites exposed improving due to the significant contribution of GO nanosheets. The energy gap of the allowed and forbidden indirect transition of PMMA-PVA/GO), also was improved by decreasing the values even with low ratio concentrations of GO nanosheets in the nanocomposites. These nanocomposites were prepared first for the first time and the results presented a good ability of the nanocomposites to adsorb the radiation. Therefore, it presented a could absorption for gamma-ray and could use as a radiation shielding application as well as, it could be promising for other applications such as filters ultraviolet, solar cell, specific optoelectronic applications, light diffusion, automotive industry, and smartphones.

Availability of data and materials

We confirm that all data and materials are authentic and available.

Authors' contributions

MA and EA performed all the experiments and data analysis. MA wrote the manuscript, contributed to the optical properties of the research and data examination. EA participated in the conception of the experiment, improved the quality of the manuscript, FTIR, OM, AFM, and SEM images. Both the authors read and approved the final manuscript.

Acknowledgements

The authors gratefully acknowledge the MSE at the University of Sheffield, the UK, composites, and materials group at the department of physics, the University of Babylon, the nanomaterials center in the Ministry of Higher education and scientific research, Iraq for their support.

Declaration of Conflicting Interests

The author(s) declared no potential conflicts of interest with respect to the research, authorship, and/or publication of this article.

Funding

The author(s) received no financial support for the research, authorship, and/or publication of this article.

ORCID iD

Ehssan Al-Bermany https://orcid.org/0000-0002-7341-623X

Supplemental material

Supplemental material for this article is available online.

References

1. Dhillon A and Kumar D. Recent advances and perspectives in polymer-based nanomaterials for Cr (VI) removal. In: *New polymer nanocomposites for environmental remediation*. Amsterdam, Netherlands: Elsevier, 2018, pp.29–46.
2. Yang J, Yan X, Wu M, et al. Self-assembly between graphene sheets and cationic poly (methyl methacrylate) (PMMA) particles: preparation and characterization of PMMA/graphene composites. *J Nanopart Res* 2012; 14: 717.
3. Molaei P and Kazeminezhad I. One-step in situ synthesis of antimony sulfide/reduced graphene oxide composite as an absorber layer with enhanced photocurrent performances for solar cells. *J Nanopart Res* 2019; 21: 1–12.
4. Abdulridha AR, Al-Bermany E, Hashim FS, et al. Synthesis and characterization and pelletization pressure effect on the properties of Bi1.7Pb0.3Sr2W0.2 Ca2Cu3 O10+δ superconductor system. *Intermetallics* 2020; 127: 106967–106968.
5. Al-Nesrawya SH, Mohseenb MJ and Al-Bermany E. Reinforcement the mechanical properties of (NR50/SBRs50/OSP) composites with oyster shell powder and carbon black. *IOP Conf Ser: Mater Sci Eng* 2020; 871: 012060–012061.
6. Firdaus RM, Rosli NIM, Ghanbaja J, et al. Enhanced adsorption of methylene blue on chemically modified graphene nanoplatelets thanks to favorable interactions. *J Nanopart Res* 2019; 21: 1–8.
7. Rashid A-KJ, Jawad ED and Kadem BY. A study of some mechanical properties of Iraqi palm fiber-PVA composite by ultrasonic. *Eur J Sci Res* 2011; 61: 203–209.
8. Smith CTG, Rhodes RW, Beliatis MJ, et al. Graphene oxide hole transport layers for large area, high efficiency organic solar cells. *Appl Phys Lett* 2014; 105: 073304–073305.
9. Abdelamir AI, Al-Bermany E and Hashim FS. Important factors affecting the microstructure and mechanical properties of PEG/GO-based nanographene composites fabricated applying assembly-acoustic method. *AIP Conf Proc* 2020; 2213: 020110.
10. Cao C, Daly M, Singh CV, et al. High strength measurement of monolayer graphene oxide. *Carbon* 2015; 81: 497–504.
11. Abdelamir AI, Al-Bermany E and Hashim FS. Enhance the optical properties of the synthesis PEG/graphene-based nanocomposite films using GO nanosheets. *J Phys: Conf Ser* 2019; 1294: 022029–022021.
12. Abdul M and Al-Bermany E. Enhance the electrical properties of the novel fabricated PMMA-PVA/graphene based nanocomposites. *J Green Eng* 2020; 10: 3465–3483.
13. Yun YS, Kim DH, Kim B, et al. Transparent conducting films based on graphene oxide/silver nanowire hybrids with high flexibility. *Synth Metals* 2012; 162: 1364–1368.
14. Hasan MT, Senger BJ, Ryan C, et al. Optical band gap alteration of graphene oxide via ozone treatment. *Sci Rep* 2017; 7: 1–8.
15. Kausor M, Al and Chakrabortty D. Optimization of system parameters and kinetic study of photocatalytic

degradation of toxic acid blue 25 dye by Ag3PO4@RGO nanocomposite. *J Nanopart Res* 2020; 22: 1–17.
16. Mirakhory M, Khatibi MM and Sadeghzadeh S. Nanoparticle mass detection by single-layer triangular graphene sheets, the extraordinary geometry for detection of nanoparticles. *J Nanopart Res* 2020; 22: 1–19.
17. Kutz M. *Handbook of materials selection*. Hoboken, NJ: John Wiley&Sons, 2002.
18. Ezrin M. *Plastics failure guide: cause and prevention*. Munich, Germany: Hanser Publishers, 1996, 473p.
19. Rajendran S, Sivakumar M and Subadevi R. Investigations on the effect of various plasticizers in PVA-PMMA solid polymer blend electrolytes. *Mater Lett* 2004; 58: 641–649.
20. Nakamura Y, Kariya E, Fukuda T, et al. Glass transition behaviour of PMMA/PVA incompatible blend. *Polym Polym Compos* 2013; 21: 367–376.
21. Sivakumar M, Subadevi R, Rajendran S, et al. Electrochemical studies on [(1 – *x*)PVA-*x*PMMA] solid polymer blend electrolytes complexed with LiBF4. *Mater Chem Phys* 2006; 97: 330–336.
22. Tripathi J, Tripathi S, Sharma A, et al. Effect of PVA concentration on bond modifications in PVA-PMMA blend films. In: *AIP conference proceedings*, 2016, vol. 1731, pp. 1–3.
23. Yakuphanoglu F and Erten H. Refractive index dispersion and analysis of the optical constants of an ionomer thin film. *Opt Appl* 2005; 35: 969–976.
24. Ravindra C, Sarswati M, Sukanya G, et al. Tensile and thermal properties of poly (vinyl) pyrrolidone/vanillin incorporated polyvinyl alcohol films. *Res J Phys Sci* 2015; 3: 1–6.
25. Jawad ED, Khudhair SHSH and Ali HNHN. A thermodynamic study of adsorption of some days on Iraqi bentoniet modified clay. *Eur J Sci Res* 2011; 60: 63–70.
26. Lee JH, Lee HB and Andrades JD. Blood compatibility of polyethylene oxide surfaces. *Prog Polym Sci* 1995; 20:1043–1079.
27. Qiu K and Netravali AN. Fabrication and characterization of biodegradable composites based on microfibrillated cellulose and polyvinyl alcohol. *Compos Sci Technol* 2012; 72: 1588–1594.
28. Qiu K and Netravali AN. A composting study of membrane-like polyvinyl alcohol based resins and nanocomposites. *J Polym Environ* 2013; 21: 658–674.
29. Guo Z, Zhang D, Wei S, et al. Effects of iron oxide nanoparticles on polyvinyl alcohol: interfacial layer and bulk nanocomposites thin film. *J Nanopart Res* 2010; 12: 2415–2426.
30. Gautam A and Ram S. Preparation and thermomechanical properties of Ag-PVA nanocomposite films. *Mater Chem Phys* 2010; 119: 266–271.
31. Zhao X, Zhang Q, Chen D, et al. Enhanced mechanical properties of graphene-based polyvinyl alcohol composites. *Macromolecules* 2010; 43: 2357–2363.
32. Rajabi M, Mahanpoor K and Moradi O. Preparation of PMMA/GO and PMMA/GO-Fe 3 O 4 nanocomposites for malachite green dye adsorption: kinetic and thermodynamic studies. *Composites Part B* 2019; 167: 544–555.
33. Rissanou AN and Harmandaris V. Structure and dynamics of poly(methyl methacrylate)/graphene systems through atomistic molecular dynamics simulations. *J Nanopart Res* 2013; 15: 1–14.
34. Al-Bermany E. *Polymer/graphene oxide nanocomposites: surface adsorption and interfaces*. Doctoral Dissertation, University of Sheffield, UK, 2017.
35. Al-Bermany E and Chen B. Preparation and characterisation of poly(ethylene glycol)-adsorbed graphene oxide nanosheets. *Polym Int* 2021; 70: 341–351.
36. Alias AN, Zabid ZM, Ali AMM, et al. Optical characterization and properties of polymeric materials for optoelectronic and photonic applications. *Int J Appl Sci Technol* 2013; 3: 11–38.
37. Pankove JI. *Optical processes in semiconductors*. New York, NY: Dover Publications, Inc., 1971.
38. Maria TMC, De Carvalho RA, Sobral P, et al. The effect of the degree of hydrolysis of the PVA and the plasticizer concentration on the color, opacity, and thermal and mechanical properties of films based on PVA and gelatin blends. *J Food Eng* 2008; 87: 191–199.
39. Suryawanshi VN, Varpe AS and Deshpande MD. Band gap engineering in PbO nanostructured thin films by Mn doping. *Thin Solid Film* 2018; 645: 87–92.
40. Tintu R, Saurav K, Sulakshna K, et al. Ge28Se60Sb12/PVA composite films for photonic applications. *J Non-Oxide Glasses* 2010; 2: 167–174.
41. Atta ER, Zk M and Madbouly AM. Research article study on polymer clay layered nanocomposites as shielding materials for ionizing radiation. *Int J Recent Sci Res* 2015; 6: 4263–4269.
42. Vijayakumari G, Selvakumar N, Jeyasubramanian K, et al. Investigation on the electrical properties of polymer metal nanocomposites for physiological sensing applications. *Phys Proc* 2013; 49: 67–78.
43. Luo Q, Shan Y, Zuo X, et al. Anisotropic tough poly (vinyl alcohol)/graphene oxide nanocomposite hydrogels for potential biomedical applications. *RSC Adv* 2018; 8: 13284–13291.
44. Tripathi J, Tripathi S, Sharma A, et al. Effect of PVA concentration on bond modifications in PVA- PMMA blend films. *AIP Conf Proc* 2016; 1731: 1–4.
45. Zheng L and Zhen W. Surface functionalization of graphene oxide via activators regenerated by electron transfer for atom transfer radical polymerization and its effect on the performance of poly(lactic acid). *Polymer (Korea)* 2018; 42: 581–593.
46. Hummers WS and Offeman RE. Preparation of graphitic oxide. *J Am Chem Soc* 1958; 80: 1339.
47. Rameshkumar C, Sarojini S, Naresh K, et al. Preparation and characterization of pristine PMMA and PVDF thin film using solution casting process for optoelectronic devices. *J Surf Sci Technol* 2017; 33: 12–18.
48. Wang C, Feng L, Yang H, et al. Graphene oxide stabilized polyethylene glycol for heat storage. *Phys Chem Chem Phys* 2012; 14: 13233–13238.
49. Fu Y, Xiong W, Wang J, et al. Polyethylene glycol based graphene aerogel confined phase change materials with

high thermal stability. *J Nanosci Nanotechnol* 2018; 18: 3341–3347.
50. Yang Z, Zhang Y and Wen B. Enhanced electromagnetic interference shielding capability in bamboo fiber@polyaniline composites through microwave reflection cavity design. *Compos Sci Technol* 2019; 178: 41–50.
51. Qiu M, Zhang Y and Wen B. Facile synthesis of polyaniline nanostructures with effective electromagnetic interference shielding performance. *J Mater Sci: Mater Electron* 2018; 29: 10437–10444.
52. Indolia AP and Gaur MS. Optical properties of solution grown PVDF-ZnO nanocomposite thin films. *J Polym Res* 2013; 20: 1–8.
53. Chang H and Wu H. Graphene-based nanocomposites: preparation, functionalization, and energy and environmental applications. *Energy Environ Sci* 2013; 6: 3483–3507.
54. Search H, Journals C, Contact A, et al. Optical, dielectric and electrical properties of PVA doped with Sn nanoparticles. *Mater Res Exp* 2014; 1: 025024.
55. Feng Y, Dong N, Wang G, et al. Saturable absorption behavior of free-standing graphene polymer composite films over broad wavelength and time ranges. *Opt Express* 2015; 23: 559–559.
56. Barroso-Bujans F, Fernandez-Alonso F, Cerveny S, et al. Two-dimensional subnanometer confinement of ethylene glycol and poly(ethylene oxide) by neutron spectroscopy: molecular size effects. *Macromolecules* 2012; 45: 3137–3144.
57. Phukan P and Saikia D. Optical and structural investigation of CdSe quantum dots dispersed in PVA matrix and photovoltaic applications. *Int J Photoenergy* 2013; 2013: 1–6.
58. Fortunati E, Luzi F, Puglia D, et al. Processing of PLA nanocomposites with cellulose nanocrystals extracted from *Posidonia oceanica* waste: innovative reuse of coastal plant. *Indus Crops Prod* 2015; 6767: 439–447.
59. Feng Y, Zhang X, Shen Y, et al. A mechanically strong, flexible and conductive film based on bacterial cellulose/graphene nanocomposites. *Carbohydr Polym* 2012; 87: 644–649.
60. Al-Bermany E, Qais D and Al-Rubaye S. Graphene effect on the mechanical properties of poly (ethylene oxide)/graphene oxide nanocomposites using ultrasound technique. *J Phys Conf Ser* 2019; 1–12.